INTERNATIONAL JOURNAL FOR NUMERICAL METHODS IN ENGINEERING
Int. J. Numer. Meth. Engng 2015; **103**:430–444
Published online 19 March 2015 in Wiley Online Library (wileyonlinelibrary.com). DOI: 10.1002/nme.4898

A new formulation for imposing Dirichlet boundary conditions on non-matching meshes

Aurelia Cuba Ramos[1], Alejandro M. Aragón[2,*,†], Soheil Soghrati[3], Philippe H. Geubelle[4] and Jean-François Molinari[1]

[1]*Civil Engineering Institute, Materials Science and Engineering Institute, École Polytechnique Fédérale de Lausanne (EPFL), Station 18 CH-1015 Lausanne, Switzerland*
[2]*Department of Precision and Microsystems Engineering, Faculty of 3mE, Delft University of Technology, Mekelweg 2, 2628 CD, Delft, The Netherlands*
[3]*Department of Mechanical and Aerospace Engineering, The Ohio State University, 201 West 19th Avenue, Columbus, OH 43210, USA*
[4]*Aerospace Engineering Department, University of Illinois, 104 South Wright Street, Urbana, IL 61801, USA*

SUMMARY

Generating matching meshes for problems with complex boundaries is often an intricate process, and the use of non-matching meshes appears as an appealing solution. Yet, enforcing boundary conditions on non-matching meshes is not a straightforward process, especially when prescribing those of Dirichlet type. By combining a type of Generalized Finite Element Method (GFEM) with the Lagrange multiplier method, a new technique for the treatment of essential boundary conditions on non-matching meshes is introduced in this manuscript. The new formulation yields a symmetric stiffness matrix and is straightforward to implement. As a result, the methodology makes possible the analysis of problems with the use of simple structured meshes, irrespective of the problem domain boundary. Through the solution of linear elastic problems, we show that the optimal rate of convergence is preserved for piecewise linear finite elements. Yet, the formulation is general and thus it can be extended to other elliptic boundary value problems. Copyright © 2015 John Wiley & Sons, Ltd.

Received 24 December 2013; Revised 19 January 2015; Accepted 26 January 2015

KEY WORDS: GFEM; XFEM; IGFEM; Lagrange multiplier method; Dirichlet boundary conditions; non-matching meshes

1. INTRODUCTION

The modeling of many problems in physics and engineering involves complex geometries. The analysis of these problems by means of the standard Finite Element Method (FEM) is often an intricate process. This complexity stems from the fact that accurate FEM solutions can only be obtained by using meshes that conform to the boundary of the problem domain. In this paper, *conforming mesh* and *matching mesh* are used interchangeably, denoting that the faces of finite elements align with the geometric boundaries of the objects they discretize. Generating conforming meshes for complex geometries is indeed challenging, especially in three dimensions. Even though significant progress has been made in the development of efficient mesh-generation software, creating matching meshes remains a laborious process that is associated with high computational costs. Further issues arise if the problem domain contains strong or weak discontinuities, *i.e.*, C^{-1}-continuous and C^0-continuous solution fields, respectively. In such cases, the Finite Element (FE) mesh needs to conform not only to the external boundary but also to the geometry of the discontinuities, which makes the mesh generation even more challenging.

*Correspondence to: Alejandro M. Aragón, Department of Precision and Microsystems Engineering, Faculty of 3mE, Delft University of Technology, Mekelweg 2, 2628 CD, Delft, The Netherlands.
†E-mail: a.m.aragon@tudelft.nl

The limitations of the standard FEM with the use of matching meshes become particularly apparent when dealing with problems where boundaries change throughout the analysis. In these problems, re-meshing in every step of the analysis is required, and thus, a completely different approach is necessary.

The Generalized/eXtended Finite Element Method (GFEM/XFEM) addresses these problems by incorporating especial enrichment functions to the standard FE basis [1–5]. In the following, the terminology GFEM will be used to refer to both the GFEM and the XFEM as they are essentially the same method [6]. The enrichment functions incorporate *a priori* knowledge of the solution field and therefore make possible the obtention of accurate solutions using non-matching meshes. According to the particular problem at hand, different types of enrichment functions have been successfully applied with the GFEM. Examples of enrichment functions are numerous and include harmonic polynomials, the Heaviside function for strong discontinuities, the level set function for weak discontinuities, closed-form solutions for dislocations in infinite media, and the asymptotic solution of Williams for crack tip fields [3, 7–9]. The method is consequently applicable to a wide range of problems, and in many cases, simple structured meshes are used in the analysis. The fact that the mesh can be chosen independently of the problem geometry is a major advantage of the method. The solutions obtained with the GFEM preserve the optimal convergence rate if a proper enrichment function is chosen, while offering greater flexibility compared to the FEM. Successful GFEM applications include the modeling of crack growth [10, 11], solidification problems [12], two-phase fluids [13], contact [14], and multiscale analysis [15]. A comprehensive review of the method and its applications can be found in [16].

Even though the GFEM offers many advantages compared with the standard FEM, the treatment of Dirichlet boundary conditions (BCs) in the former poses significant problems if the FE mesh does not align with the Dirichlet boundary. The problem is similar to the treatment of Dirichlet BCs in mesh-free methods, as there is no way to strongly enforce Dirichlet BCs in the GFEM. This is because test functions, which vanish only on the Dirichlet boundary, are very difficult to construct without over-constraining the problem and causing boundary locking [17–19]. In this case, the approximation of the normal flux is sub-optimal, as discussed by Moës *et al.* [19]. The most common ways for imposing Dirichlet BCs on non-matching meshes are the use of Lagrange multipliers [19–25], Nitsche's method [22, 26, 27], the penalty method [22, 28], and hybrid/discontinuous Galerkin formulations [29, 30]. Among these techniques, the Lagrange multiplier method can be applied to a large set of problems for which the solution requires constraints to be satisfied. In its straightforward formulation, the Lagrange multiplier is introduced as a dual field, in addition to the primal unknown field. However, the choice of an appropriate Lagrange multiplier space is complex. In many cases, oscillations in the tractions along the Dirichlet boundary are observed, indicating that boundary locking occurs [19, 31, 32]. This can be explained mathematically by the fact that the inf-sup condition is not satisfied [33]. Approaches to resolve this issue can be classified into three main categories. Methods in the first category make use of additional stabilizing terms and are therefore known as *stabilized* methods. The work of Barbosa and Hughes [25] is one of the earliest contributions in this category. The authors guaranteed stability of the Lagrange multiplier method by adding least squares-like terms to the Galerkin formulation. Another stabilized method was proposed by Burman and Hansbo [24], by combining element-wise constant multipliers with a stabilizing parameter to penalize the jump of the multiplier over element faces. Recently, Hautefeuille *et al.* [23] used a Nitsche-type variational approach for stabilization of the Lagrange multipliers. In contrast to stabilized techniques, the methods in the second and third categories are referred to as *stable* because they do not require an additional stabilization term. In the second category, stability is ensured by choosing a number of Lagrange multipliers that is small enough to pass the inf-sup test. In order to build such a reduced Lagrange multiplier space, Moës *et al.* [19] proposed a complex algorithm to select a set of nodes on which independent Lagrange multipliers can be defined. A more straightforward algorithm to detect these so-called vital vertices was outlined in [34], where the space was obtained by applying the trace operator to the primary shape functions. Hautefeuille *et al.* [23] combined this algorithm with a new discontinuous set of shape functions for the Lagrange multipliers. Finally, the stable Lagrange multiplier methods in the third category ensure stability by enriching the primal space.

DOI: 10.1002/nme

This approach was used by Gerstenberger and Wall [20], who shifted the constraining multiplier field from the interface to the background mesh. The Lagrange multiplier field was consequently replaced by an additional unknown stress field. They enriched both the primal and the additional stress fields with a step function to ensure stability. The new methodology presented in this paper makes use of an enriched primal field as well and hence belongs to the last category.

In this work, we show that Dirichlet BCs on nodes of enriched elements in non-matching FE meshes can be enforced by coupling the Lagrange multiplier method to the Interface-enriched Generalized Finite Element Method (IGFEM). The IGFEM is a special type of GFEM that was introduced recently for the treatment of weak discontinuities [35]. It has been successfully applied to the treatment of heat transfer problems in two dimensions [35] and three dimensions [36], to the conjugate heat transfer problem in microvascular polymeric materials [37, 38], and to the cohesive failure of heterogeneous adhesives [39]. The IGFEM enrichment function vanishes at the standard nodes of enriched elements by construction. This is an important property that allows for a straightforward imposition of Dirichlet BCs on enriched elements that conform to the Dirichlet boundary. We demonstrate that this property is also advantageous for the treatment of Dirichlet BCs on enriched elements that do not conform to the essential boundary. An immediate consequence of the IGFEM formulation is the explicit discretization of the boundary, which can conveniently be used for the definition of a Lagrange multiplier space. Following the method proposed by Ferández-Méndez and Huerta [22] for the imposition of Dirichlet BCs in mesh-free methods, we use the point collocation method for the construction of the aforementioned space. To our knowledge, this is the first work that combines the point collocation method with a generalized FE formulation for prescribing Dirichlet BCs on non-matching meshes. With this approach, no oscillations in the multiplier are encountered, and thus, stabilization of the Lagrange multiplier is not required. The proposed method is straightforward to implement, and the results show that the optimal rate of convergence is preserved.

The remainder of this paper is organized as follows. In Section 2, the problem formulation is outlined. The weak form is then discretized, and the properties of the final system of equations are discussed. Subsequently, in Section 3, the results for various examples of linear elasticity are analyzed, and a convergence study is presented. Finally, conclusions are given in Section 4.

2. PROBLEM FORMULATION

Consider the d-dimensional ($d = 2, 3$) Euclidean space $\mathbb{R}^d$, where a coordinate is given by $\boldsymbol{x} = x_i \boldsymbol{e}_i$, and $\boldsymbol{e}_i$ are the vectors of a chosen basis (Figure 1). Let $\Omega \subset \mathbb{R}^d$, with closure $\overline{\Omega}$, represent

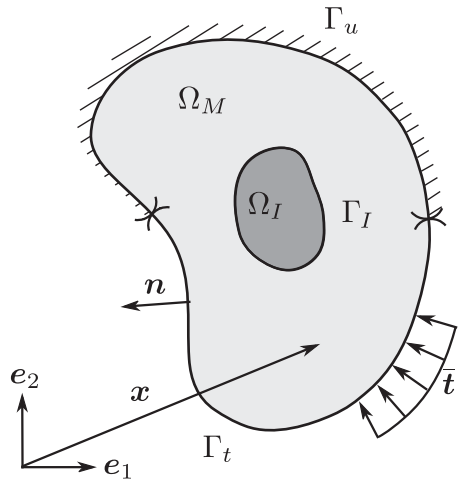

Figure 1. Mathematical representation of a solid Ω, composed of matrix and inclusion phases Ω_M and Ω_I, respectively. Regions of the boundary Γ_u and Γ_t represent the portions of the boundary with prescribed Dirichlet and Neumann boundary conditions.

DOI: 10.1002/nme

a solid composed of two mutually exclusive phases Ω_M and Ω_I that indicate the matrix and the inclusion, respectively. The domain boundary $\Gamma \equiv \partial\Omega$ consists of the Dirichlet boundary Γ_u and the Neumann boundary Γ_t, such that $\overline{\Gamma} = \overline{\Gamma}_u \cup \overline{\Gamma}_t$ and $\Gamma_u \cap \Gamma_t = \emptyset$. The outward unit normal to Γ is thus $\boldsymbol{n} = n_i \boldsymbol{e}_i$. The material interface is denoted with $\Gamma_I = \overline{\Omega}_M \cap \overline{\Omega}_I$.

The strong form of the boundary value problem is as follows: Given the body force $\boldsymbol{b} : \Omega \to \mathbb{R}^d$, the Cauchy stress tensor $\boldsymbol{\sigma} : \overline{\Omega} \times \overline{\Omega} \to \mathbb{R}^d$, the prescribed displacement $\bar{\boldsymbol{u}} : \Gamma_u \to \mathbb{R}^d$, and the prescribed traction $\bar{\boldsymbol{t}} : \Gamma_t \to \mathbb{R}^d$, find the displacement field $\boldsymbol{u} : \overline{\Omega} \to \mathbb{R}^d$ such that

$$\nabla \cdot \boldsymbol{\sigma} + \boldsymbol{b} = \boldsymbol{0} \qquad \text{in } \Omega_M, \Omega_I, \tag{1}$$

$$\boldsymbol{\sigma} \cdot \boldsymbol{n} = \bar{\boldsymbol{t}} \qquad \text{on } \Gamma_t, \tag{2}$$

$$\boldsymbol{u} = \bar{\boldsymbol{u}} \qquad \text{on } \Gamma_u, \tag{3}$$

with bimaterial interface conditions

$$[\![\boldsymbol{\sigma} \cdot \boldsymbol{n}]\!] = \boldsymbol{0} \qquad \text{on } \Gamma_I, \tag{4}$$

$$[\![\boldsymbol{u}]\!] = \boldsymbol{0} \qquad \text{on } \Gamma_I. \tag{5}$$

In Equation (1), $\nabla\cdot$ denotes the divergence operator, and $[\![\cdot]\!]$ in Equations (4) and (5) denotes the jump across the material interface, *i.e.*, $[\![\boldsymbol{\varphi}]\!] = \boldsymbol{\varphi}|_{\Gamma_I^+} - \boldsymbol{\varphi}|_{\Gamma_I^-}$ for some vector-valued function $\boldsymbol{\varphi}$. In addition, the explicit dependence of the Cauchy stress tensor on the displacement field has been omitted, *i.e.*, $\boldsymbol{\sigma} = \tilde{\boldsymbol{\sigma}}(\boldsymbol{u})$.

Let $\mathcal{U}(\Omega) := \left\{ \boldsymbol{u} : \overline{\Omega} \to \mathbb{R}^d \,\middle|\, u_i \in \mathcal{H}^1(\Omega),\ i = 1, \ldots, d \right\}$ be the set of functions used for the trial solution and the weight functions, where $\mathcal{H}^1(\Omega)$ denotes the Hilbert–Sobolev first-order space [40]. Furthermore, let $\mathcal{L}(\Gamma_u) := \left\{ \boldsymbol{\eta} \,\middle|\, \eta_i \in \mathcal{H}^{-1/2}(\Gamma_u) \right\}$ be the set of functions used for the Lagrange multiplier field introduced to enforce the Dirichlet BC (3), where $\mathcal{H}^{-1/2}(\Gamma_u)$ denotes the dual space of $\mathcal{H}^{1/2}(\Gamma_u)$ [41]. The resulting weak form of the problem can be written as follows: Find $\boldsymbol{u} \in \mathcal{U}$ and $\boldsymbol{\eta} \in \mathcal{L}(\Gamma_u)$ such that

$$a(\boldsymbol{v}, \boldsymbol{u})_\Omega - (\boldsymbol{\gamma}, \boldsymbol{u} - \bar{\boldsymbol{u}})_{\Gamma_u} - (\boldsymbol{v}, \boldsymbol{\eta})_{\Gamma_u} = (\boldsymbol{v}, \bar{\boldsymbol{t}})_{\Gamma_t} + (\boldsymbol{v}, \boldsymbol{b})_\Omega \qquad \forall\, \boldsymbol{v} \in \mathcal{U}(\Omega), \boldsymbol{\gamma} \in \mathcal{L}(\Gamma_u). \tag{6}$$

The bilinear and linear forms are defined as follows:

$$\begin{aligned}
a(\boldsymbol{v}, \boldsymbol{u})_\Omega &= \int_\Omega \boldsymbol{\sigma}(\boldsymbol{u}) : \boldsymbol{\varepsilon}(\boldsymbol{v})\, d\Omega, \\
(\boldsymbol{\gamma}, \boldsymbol{u} - \bar{\boldsymbol{u}})_{\Gamma_u} &= \int_{\Gamma_u} \boldsymbol{\gamma} \cdot (\boldsymbol{u} - \overline{\boldsymbol{u}})\, d\Gamma, \\
(\boldsymbol{v}, \boldsymbol{\eta})_{\Gamma_u} &= \int_{\Gamma_u} \boldsymbol{v} \cdot \boldsymbol{\eta}\, d\Gamma, \\
(\boldsymbol{v}, \bar{\boldsymbol{t}})_{\Gamma_t} &= \int_{\Gamma_t} \boldsymbol{v} \cdot \bar{\boldsymbol{t}}\, d\Gamma, \\
(\boldsymbol{v}, \boldsymbol{b})_\Omega &= \int_\Omega \boldsymbol{v} \cdot \boldsymbol{b}\, d\Omega,
\end{aligned}$$

where $\boldsymbol{\varepsilon}$ denotes the infinitesimal strain tensor

$$\boldsymbol{\varepsilon} = \nabla_S \boldsymbol{u} = \frac{1}{2}\left(\nabla \boldsymbol{u} + \nabla \boldsymbol{u}^{\mathrm{T}}\right). \tag{7}$$

Note that the Lagrange multiplier field has a physical interpretation, as it defines the mechanical traction $\boldsymbol{\eta} = \boldsymbol{\sigma} \cdot \boldsymbol{n}$ along the Dirichlet boundary [22]. Note also that the Dirichlet BC is enforced in a weak sense.

In the following, it is assumed that an arbitrary d-dimensional domain $\mathcal{D}$, on which the mesh will be constructed, may be larger than the actual problem domain Ω, *i.e.*, $\Omega \subseteq \mathcal{D}$ (Figure 2(a)). The domain $\mathcal{D}$ is called the *hold-all domain* [17] and is discretized into n_{el} finite elements such that $\mathcal{D}^h \equiv \operatorname{int}\left(\cup_{i=1}^{n_{el}} \overline{\omega}_i\right)$ and $\omega_i \cap \omega_j = \emptyset, \forall i \neq j$. Note that $\mathcal{D} \equiv \mathcal{D}^h$ because the hold-all

DOI: 10.1002/nme

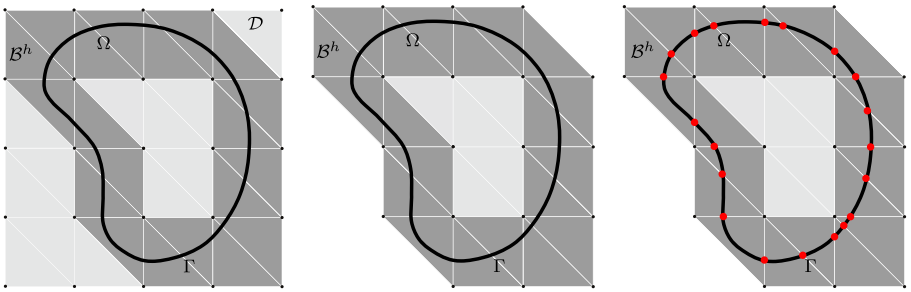

Figure 2. (a) Hold-all domain $\mathcal{D}$ that contains the actual problem domain Ω and its boundary Γ. The element set $\mathcal{B}^h$ consists of all finite elements that have a non-empty intersection with Γ; (b) elements that lie fully outside the problem domain are removed from the analysis; and (c) red circles denote the location of additional nodes that are created along the boundary for the IGFEM formulation.

domain is chosen to have a simple boundary in order to ease the generation of a structured mesh. The boundary sub-mesh is defined as $\mathcal{B}^h := \{\cup_i \omega_i |\ \omega_i \cap \Gamma \neq \emptyset\}$. The cardinality of $\mathcal{B}^h$ is denoted by n_B, *i.e.*, the number of elements in the set $\mathcal{B}^h$. All elements for which $\omega_i \cap \Omega = \emptyset$ lie fully outside the problem domain and are therefore discarded during the analysis (Figure 2(b)). The focus in this paper is on the treatment of the elements contained in $\mathcal{B}^h$ and not on elements intersected by the bimaterial interface, which was discussed in detail in [35]. The inclusion phase is thus not explicitly shown in Figure 2(a)–2(c) to facilitate the illustration.

For the discretization of the weak form (6), appropriate approximations for the displacement and the Lagrange multiplier fields need to be chosen. The IGFEM formulation is used to discretize the displacement field [35]. Let the set $\mathcal{U}^h \subset \mathcal{H}^1(\mathcal{D})$ consist of polynomial interpolation functions of the form used in the IGFEM, *i.e.*,

$$\mathcal{U}^h(\mathcal{D}) := \left\{ \boldsymbol{u}^h(\boldsymbol{x}) = \underbrace{\sum_{i=1}^{n} N_i(\boldsymbol{x})\boldsymbol{U}_i}_{\text{standard FE part}} + \underbrace{\sum_{i=1}^{n_{en}} \Psi_i(\boldsymbol{x})\boldsymbol{\alpha}_i}_{\text{enriched part}} \right\}, \tag{8}$$

where the first term in the interpolating function involves a summation over the n nodes of the finite element mesh and the second term over n_{en} interface nodes. The latter is created during the generation of integration elements by intersecting the problem boundary and the material interface with the element edges (Figure 2(c)). In Equation (8), $N_i(\boldsymbol{x})$ denote the standard linear Lagrangian shape functions, $\boldsymbol{U}_i$ the standard degrees of freedom (DOFs), $\Psi_i(\boldsymbol{x})$ the IGFEM enrichment functions, and $\boldsymbol{\alpha}_i$ the enriched DOFs. Note that, as in the standard FEM, a geometrical discretization error is introduced when the geometry of the boundary and that of the material interface are not captured exactly, *i.e.*, $\Gamma \cong \Gamma^h$, $\Gamma_I \cong \Gamma_I^h$. Yet, this error could be reduced by adding one or more nodes over the interface [35]. The enrichment functions are obtained from a linear combination of the standard Lagrangian shape functions in the integration subdomains. In Equation (8), the Lagrangian shape functions $N_i(\boldsymbol{x})$ form a *partition of unity*, *i.e.*, they satisfy $\sum_{i=1}^{n} N_i(\boldsymbol{x}) = 1,\ \forall \boldsymbol{x} \in \mathcal{D}^h$. In the conventional GFEM formulation, the partition of unity is used to ensure that enrichment functions are localized to the elements that contain enriched DOFs. This is not needed in the IGFEM because the enrichment functions have local support by construction, so that they are identically zero on finite elements that do not interact with the interface. This fact constitutes the main difference between the GFEM and the IGFEM. The continuity of the displacement field is ensured by requiring that the $\boldsymbol{\alpha}_i$ are shared between interface nodes of neighboring integration elements. Having defined the interpolating functions for the displacement field, the difficulty now lies in the choice of a correct Lagrange multiplier set that will not trigger oscillations. As suggested in [22], the point collocation method will be used for the discretization, where the collocation points ($d = 2, 3$) are chosen such that they correspond to the nodes that are created on the intersection between the boundary and the edges of the hold-all domain mesh. In this method, the Dirac delta function $\delta(\|\boldsymbol{x}\|)$ is chosen as

DOI: 10.1002/nme

the shape function for the Lagrange multipliers. The Lagrange multiplier set $\mathcal{L}^h$ is consequently defined as follows:

$$\mathcal{L}^h(\Gamma_u) := \left\{ \boldsymbol{\eta}^h(\boldsymbol{x}) = \sum_i^{n_{en}} \delta\left(\left\|\boldsymbol{x} - \boldsymbol{x}_i^B\right\|\right) \boldsymbol{\eta}_i \right\}, \tag{9}$$

where $\boldsymbol{x}_i^B$ corresponds to the coordinates of the interface nodes on the Dirichlet boundary Γ_u.

The discrete formulation of the weak form can be formulated in the Bubnov–Galerkin setting

$$\begin{aligned} a(\boldsymbol{v}^h, \boldsymbol{u}^h)_\Omega - \left(\boldsymbol{\gamma}^h, \boldsymbol{u}^h - \overline{\boldsymbol{u}}\right)_{\Gamma_u} - \left(\boldsymbol{v}^h, \boldsymbol{\eta}^h\right)_{\Gamma_u} &= (\boldsymbol{v}^h, \boldsymbol{t})_{\Gamma_t} + (\boldsymbol{v}^h, \boldsymbol{b})_\Omega, \\ \forall \boldsymbol{v}^h \in \mathcal{U}^h, \forall \boldsymbol{\gamma}^h \in \mathcal{L}^h, & \end{aligned} \tag{10}$$

where $\boldsymbol{u}^h$ and $\boldsymbol{\eta}^h$ are defined in (8) and (9).

In order to assemble the final system of equations from the weak form (10), the enriched element shape function vector $\hat{\mathbf{N}}^{el}$ and the boundary shape function vector $\hat{\mathbf{M}}^{el}$ are defined as

$$\hat{\mathbf{N}}^{el} = \left[N_1^{el} \ \dots \ N_{\nu_{el}}^{el} \ \Psi_1^{el} \ \dots \ \Psi_{\nu_{en}}^{el}\right], \tag{11}$$

$$\hat{\mathbf{M}}^{el} = \left[\delta\left(\left\|\boldsymbol{x} - \boldsymbol{x}_1^B\right\|\right) \ \dots \ \delta\left(\left\|\boldsymbol{x} - \boldsymbol{x}_{\nu_{en}}^B\right\|\right)\right], \tag{12}$$

where ν_{el} and ν_{en} are the number of standard and interface nodes per element. The enriched element shape function matrix and the element boundary shape function matrix are obtained as

$$\mathbf{N}^{el} = \hat{\mathbf{N}}^{el} \otimes \mathbf{I}, \tag{13}$$

$$\mathbf{M}^{el} = \hat{\mathbf{M}}^{el} \otimes \mathbf{I}, \tag{14}$$

where $\mathbf{I}$ is the identity matrix and $\otimes$ denotes the Kronecker product.

Combining Equations (7) and (13) and using the Voigt notation, the element strain tensor can be expressed as

$$\boldsymbol{\varepsilon}^{el} = \nabla_S \mathbf{N}^{el} \mathbf{D}^{el} = \mathbf{B}^{el} \mathbf{D}^{el}, \tag{15}$$

where $\boldsymbol{D} = [\boldsymbol{U}, \boldsymbol{\alpha}]^\mathsf{T}$. This yields the global system of equations

$$\begin{bmatrix} \mathbf{K} & \mathbf{G}^\mathsf{T} \\ \mathbf{G} & \mathbf{0} \end{bmatrix} \begin{bmatrix} \boldsymbol{D} \\ \mathbf{H} \end{bmatrix} = \begin{bmatrix} \mathbf{f} \\ \mathbf{g} \end{bmatrix}, \tag{16}$$

where the vector $\mathbf{H}$ contains the coefficients $\boldsymbol{\eta}_i$, and the sub-matrices for a linear elastic material with material tensor $\mathbb{C}$ in Voigt notation are obtained as follows:

$$\mathbf{K} = \mathop{\mathbb{A}}_{el=1}^{n_{el}} \int_{\Omega^{el}} \mathbf{B}^{el\mathsf{T}} \mathbf{C}^{el} \mathbf{B}^{el} \, d\Omega, \tag{17}$$

$$\mathbf{f} = \mathop{\mathbb{A}}_{el=1}^{n_{el}} \left(\int_{\Gamma_t^{el}} \mathbf{N}^{el\mathsf{T}} \bar{\boldsymbol{t}} \, d\Gamma + \int_{\Omega^{el}} \mathbf{N}^{el\mathsf{T}} \boldsymbol{b} \, d\Omega \right), \tag{18}$$

$$\mathbf{G} = \mathop{\mathbb{A}}_{el=1}^{n_B} \int_{\Gamma_u^{el}} \mathbf{M}^{el\mathsf{T}} \mathbf{N}^{el} \, d\Gamma, \tag{19}$$

$$\mathbf{g} = \mathop{\mathbb{A}}_{el=1}^{n_B} \int_{\Gamma_u^{el}} \mathbf{M}^{el\mathsf{T}} \bar{\boldsymbol{u}} \, d\Gamma. \tag{20}$$

In Equations (17)–(20), $\mathbb{A}$ denotes the finite element assembly operator. A zero displacement is prescribed to nodes that belong to $\mathcal{B}^h$ but lie outside of Ω.

DOI: 10.1002/nme

3. NUMERICAL EXAMPLES AND CONVERGENCE STUDIES

This section discusses the application of the proposed methodology to problems of linear elasticity that contain a material interface. For the following examples, it is assumed that all materials are isotropic and linear elastic. The stress tensor therefore takes the form

$$\boldsymbol{\sigma} = \mathbb{C}\boldsymbol{\varepsilon} = \lambda \operatorname{tr}(\boldsymbol{\varepsilon})\mathbf{I} + 2\mu\boldsymbol{\varepsilon}, \tag{21}$$

where λ and μ are the Lamé parameters, $\operatorname{tr}(\cdot)$ denotes the trace operator, and $\mathbf{I}$ is the second-order identity tensor.

For the first three examples, the solution is compared with the standard IGFEM solution, where the mesh conforms to the external boundary but not to the material interface. In order to investigate the convergence and accuracy of the solutions, the L^2-norm and the energy norm a of the error are defined as follows (dependence of $\boldsymbol{u}$ on $\boldsymbol{x}$ implied):

$$\bar{\epsilon}_{L^2} := \frac{\|\boldsymbol{u} - \boldsymbol{u}^h\|_{L^2(\Omega)}}{\|\boldsymbol{u}\|_{L^2(\Omega)}} = \sqrt{\frac{\int_\Omega \|\boldsymbol{u} - \boldsymbol{u}^h\|^2 \, d\Omega}{\int_\Omega \|\boldsymbol{u}\|^2 \, d\Omega}}, \tag{22}$$

$$\bar{\epsilon}_a := \frac{\|\boldsymbol{u} - \boldsymbol{u}^h\|_a}{\|\boldsymbol{u}\|_a} = \sqrt{\frac{\int_\Omega (\boldsymbol{\varepsilon} - \boldsymbol{\varepsilon}^h) \cdot \mathbb{C}(\boldsymbol{\varepsilon} - \boldsymbol{\varepsilon}^h) \, d\Omega}{\int_\Omega \boldsymbol{\varepsilon} \cdot \mathbb{C}\boldsymbol{\varepsilon} \, d\Omega}}. \tag{23}$$

The simulation results will show that the method presented in this paper is versatilely applicable to any arbitrary boundary geometry. Furthermore, it will be demonstrated that Dirichlet and Neumann BCs can be imposed on the same node for two different DOFs.

In the last example, a thin epoxy film is deformed by applying a shear displacement along its top boundary. The geometry of the outer boundary is complex because of the roughness of the film. This last example demonstrates how the analysis is simplified by using a non-conforming mesh.

3.1. Two-dimensional plate: patch test

For the patch test, the 2D plate of size $L \times L$ depicted in Figure 3 is considered (with $L = 2$ and unit thickness). This problem, which consists of two different materials with the interface along the line $x_1 = 0$, is designed such that a 1D exact solution can be obtained in 2D. The two materials

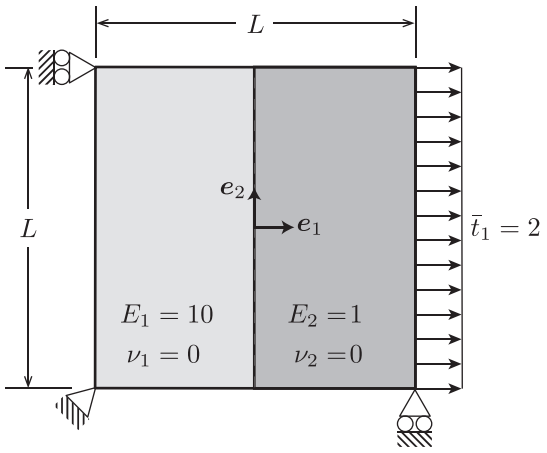

Figure 3. Two-dimensional plate on rollers. The material on the right and left sides has Young's moduli of 1 and 10, respectively. The Poisson ratio is 0 for both materials. A uniform traction $\bar{t}_1 = 2$ is applied along the right edge of the plate.

DOI: 10.1002/nme

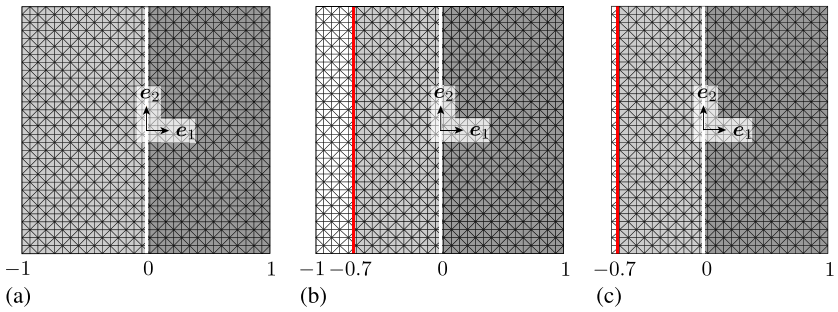

Figure 4. Finite element meshes: The white line indicates the location of the material interface and the red line the location of the part of the Dirichlet boundary that does not conform to the element edges. (a) Structured mesh that conforms to the Dirichlet boundary for standard IGFEM solution; (b) discretization of hold-all domain; and (c) structured non-conforming mesh for the IGFEM solution coupled with Lagrange multipliers.

are linear elastic, with Young's moduli taking values $E_1 = 10$ and $E_2 = 1$ for the material on the left and right sides of the interface, respectively. The Poisson ratio is equal to 0 for both materials. The displacements $\overline{u}_1 = 0$ and $\overline{u}_2 = 0$ are prescribed along the left and bottom edges, respectively. A constant traction per unit length $\overline{t}_1 = 2$ is applied along the right edge of the plate. The exact solution for the displacement field is given by

$$u_1 = \begin{cases} \frac{\overline{t}_1 x_1}{E_1} + \frac{\overline{t}_1 L}{2E_1} \text{ for } -L/2 \leqslant x_1 \leqslant 0, \\ \frac{\overline{t}_1 x_1}{E_2} + \frac{\overline{t}_1 L}{2E_1} \text{ for } \quad 0 \leqslant x_1 \leqslant L/2, \end{cases} \tag{24}$$

$$u_2 = 0. \tag{25}$$

The resulting displacement field is piecewise linear in x_1 and has a kink, *i.e.*, a weak discontinuity, along the material interface.

Numerical solutions are computed with both the standard IGFEM and with the method proposed in this paper. For the former, the problem domain Ω is discretized with a structured mesh that is conforming to the entire Dirichlet boundary and non-conforming to the material interface (Figure 4(a)). For the latter, the IGFEM is combined with the Lagrange multiplier method as described in Section 2. For this purpose, only the part of the plate starting at $x_1 = -0.7$ is modeled, and the exact solution for u_1 given in (24) is applied along the boundary $\Gamma_B = \{\boldsymbol{x} \mid x_1 = -0.7\}$. The first step involves meshing the hold-all domain, which is set to $L \times L$ in this example (Figure 4(b)). Subsequently, all elements that lie fully outside the problem domain are removed from the analysis. The final structured mesh shown in Figure 4(c) does not align to Γ_B, and therefore, the IGFEM enrichment functions are coupled with Lagrange multipliers in elements intersected by Γ_B. Note that u_2 is not constrained along Γ_B. This corresponds to a zero traction BC in the direction of $\boldsymbol{e}_2$. Consequently, Dirichlet and Neumann BCs are simultaneously being applied at the interface nodes discretizing this part of the boundary. Three-node triangular elements are used for the analysis. In both cases, the L^2-error is of the order of 10^{-14}, so that the exact solution is obtained not only with the standard IGFEM solution but also with the new formulation presented in this paper. As explained in Section 2, the Lagrange multiplier field corresponds to the traction along the Dirichlet boundary. In order to verify this, the sum over each component of the boundary force vector is calculated and compared with the sum over each component of the Lagrange multiplier vector. The difference is again of the order of 10^{-14}, *i.e.*, $\sum_{i=1}^{d\times n} f_i = \sum_{j=1}^{d\times n_{en}} \eta_j$. The distribution of the tractions along both edges of the plate is illustrated in Figure 5. It is worth noting that the traction field on the left edge does not seem uniform because the interface is placed at $x_1 = -0.7$, and so the measure contributing to each node along the interface is not uniform (as is the case in the right edge).

DOI: 10.1002/nme

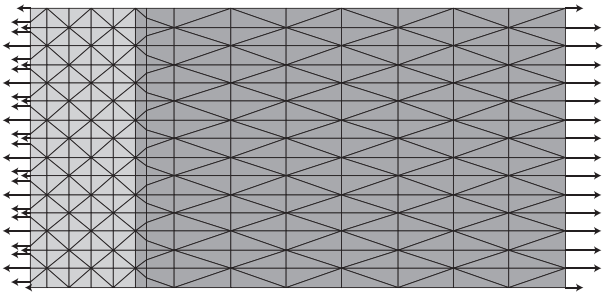

Figure 5. Deformed shape for the problem described in Section 3.1. Arrows on the right edge of the plate correspond to the applied traction, while arrows on the left edge correspond to the Lagrange multiplier in each node, *i.e.*, the resulting traction. To ease the visualization of the tractions along each edge of the plate, the traction distribution is given for the case of a coarse mesh.

3.2. Two-dimensional plate: convergence study

For the convergence study, a constant body force per unit area $b_1 = 2$ is now applied to the plate of the problem of the previous section. The exact solution for the displacement field is now given by

$$u_1 = \begin{cases} \frac{(x_1+1)\left[2\bar{t}_1 - L(x_1-3)\right]}{2E_1} & \text{for } -L/2 \leqslant x_1 \leqslant 0, \\ \frac{E_2(3L+2\bar{t}_1)+E_1 x_1\left[2(\bar{t}_1+L)-Lx_1\right]}{2E_1E_2} & \text{for } 0 \leqslant x_1 \leqslant L/2, \end{cases} \tag{26}$$

$$u_2 = 0. \tag{27}$$

Similar to the patch test, the numerical solutions are obtained with the standard IGFEM for the boundary conforming meshes and with the coupled IGFEM/Lagrange multiplier approach for meshes that do not conform to the Dirichlet boundary. In the first case, the numerical domain corresponds to the full plate, whereas in the second case, only the part of the plate for which $x_1 \geqslant -0.7$ is analyzed. The exact displacement from (26) is imposed along Γ_B in the direction of x_1. Because of the constant body force, the exact displacement field is now a quadratic function of x_1, and thus, the exact solution cannot be reproduced by using three-node triangular elements. Figure 6(a) and 6(b) shows the error in the L^2 and energy norms as a function of the mesh size h. The optimal rate of convergence is achieved with both procedures.

3.3. Eshelby inclusion problem

The second example is inspired by the classical Eshelby inclusion problem, as discussed in [8, 42, 43]. The problem domain is a circle of radius $r_u = 2$. A circular inclusion of radius $r_i = 0.4$ is embedded in the center of the domain. The material properties for the matrix and the inclusion are $E_1 = 1$, $\nu_1 = 0.25$, $E_2 = 10$, and $\nu_2 = 0.3$, respectively. Plane strain conditions are assumed, and a linear displacement is applied along the outer boundary of the domain as follows:

$$u_r(r_u, \phi) = r_u, \tag{28}$$

$$u_\theta(r_u, \phi) = 0. \tag{29}$$

The exact solution for the displacement field is given by

$$u_r(r, \phi) = \begin{cases} \left[\left(1 - \frac{r_u^2}{r_i^2}\right)\alpha + \frac{r_u^2}{r_i^2}\right] r & \text{for } 0 \leqslant r \leqslant r_i, \\ \left(r - \frac{r_u^2}{r}\right)\alpha + \frac{r_u^2}{r}, & \text{for } r_i < r \leqslant r_u, \end{cases} \tag{30}$$

$$u_\theta(r, \phi) = 0, \tag{31}$$

DOI: 10.1002/nme

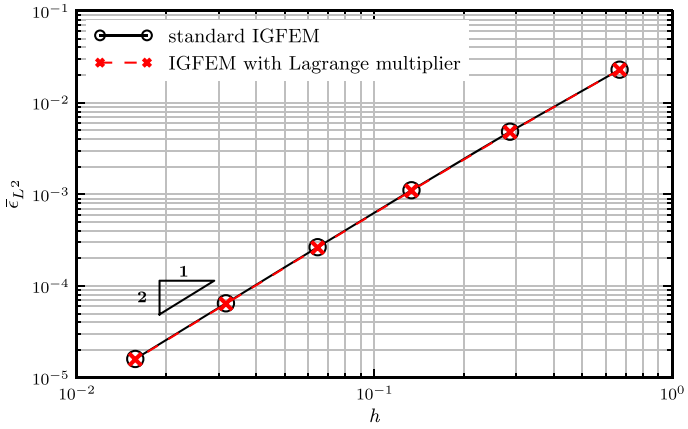

(a)

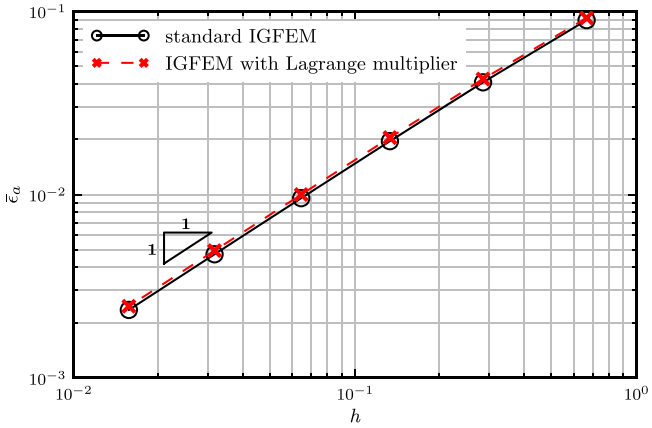

(b)

Figure 6. Convergence results for the 2D plate shown in Figure 3 with a constant body force $b_1 = 2$. The figures show the error in the L^2-norm (a) and in the energy norm (b) as a function of the mesh size h.

where α is a function of the geometry and the Lamé constants for the matrix (λ_1, μ_1) and for the inclusion (λ_2, μ_2)

$$\alpha = \frac{(\lambda_1 + \mu_1 + \mu_2) r_u}{(\lambda_2 + \mu_2) r_i^2 + (\lambda_1 + \mu_1)\left(r_u^2 - r_i^2\right) + \mu_2 r_u^2}. \tag{32}$$

Here, the numerical domain is chosen to correspond to the circular domain with radius $r_b = \sqrt{4/\pi}$ shown in Figure 7. The exact displacements are prescribed along the outer boundary of the numerical domain, and three-node triangular elements are used to construct the meshes of different levels of refinement. The problem is analyzed with the standard IGFEM and with the method introduced in this paper. The meshes are therefore conforming (Figure 8(a)) and non-conforming (Figure 8(b)) to the external boundary, respectively. The convergence results for the L^2 and energy norms are given in Figure 9(a)–9(b). Optimal rates of convergence are once again preserved.

Finally, the squared L^2-error in each element is displayed in Figure 10, where the number of elements is 1774 and 2022 for the standard IGFEM and for the IGFEM/Lagrange multiplier solutions, respectively. The Dirichlet BCs are matched exactly at boundary nodes in both cases, because the error in the elements containing the Dirichlet boundary is negligible. It can also be seen that the main source of the error corresponds to the discretization of the inner circular inclusion.

DOI: 10.1002/nme

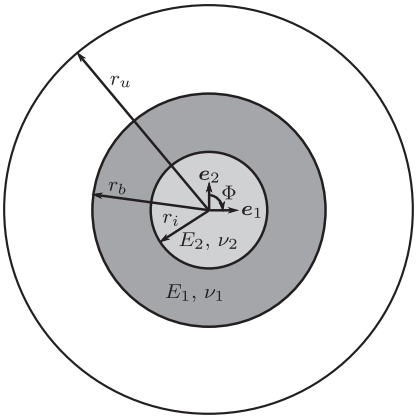

Figure 7. Eshelby inclusion problem of Section 3.3.

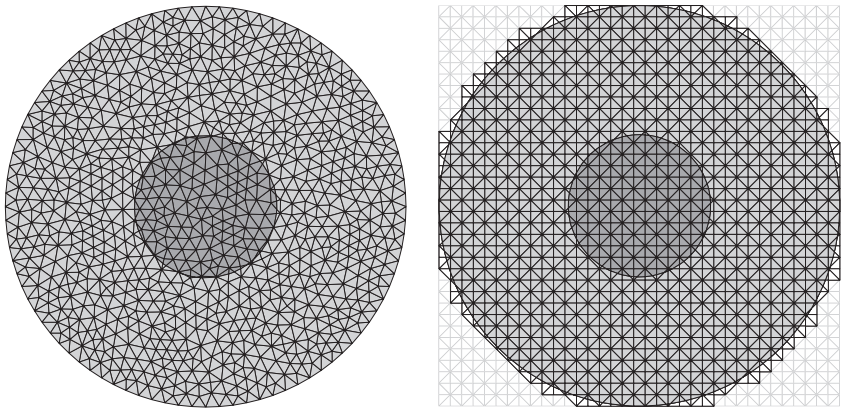

(a) looks pixelized (b) looks pixelized

Figure 8. Finite element meshes for the Eshelby inclusion problem described in Section 3.3. (a) Unstructured mesh that conforms to the Dirichlet boundary for the standard IGFEM method and (b) structured non-conforming mesh for the IGFEM solution coupled with Lagrange multipliers. The latter figure also shows the part of the hold-all domain mesh that is removed for the analysis.

3.4. Shearing of epoxy film

In this example, we study the deformation of a rough epoxy film due to an imposed shear displacement. The Young modulus and the Poisson ratio of the epoxy are 2.4 GPa and 0.34, respectively. The film has a total length of 2 mm, and the geometries of the rough bottom and top surfaces are defined by the following functions (Figure 11(a))

$$\begin{aligned} \Gamma_b &= \left\{ \boldsymbol{x} |\ x_2 - 0.001 \prod_{k=0}^{3} \sin\left(2^k 500 x_1\right) + 0.0025 = 0 \right\}, \\ \Gamma_t &= \left\{ \boldsymbol{x} |\ 0.001 \prod_{k=0}^{3} \sin\left(2^k 500 x_1\right) + 0.0025 - x_2 = 0 \right\}. \end{aligned} \tag{33}$$

The epoxy film is fixed along the bottom side, and a shear displacement, which is proportional to the height, is imposed along the top side

$$\bar{\boldsymbol{u}} = \begin{cases} \boldsymbol{0} & \forall \boldsymbol{x} \in \Gamma_b, \\ 0.3 x_2 \boldsymbol{e}_1 & \forall \boldsymbol{x} \in \Gamma_t. \end{cases} \tag{34}$$

DOI: 10.1002/nme

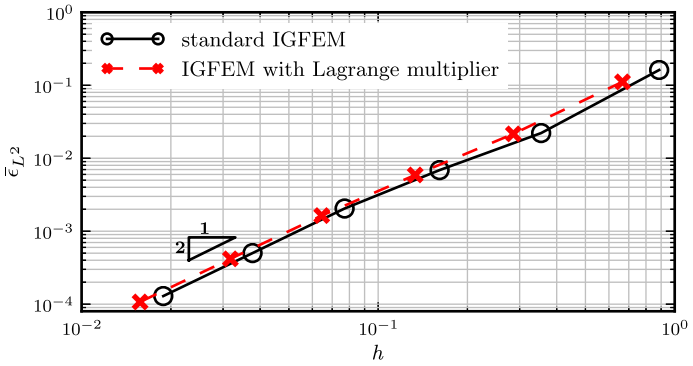

(a)

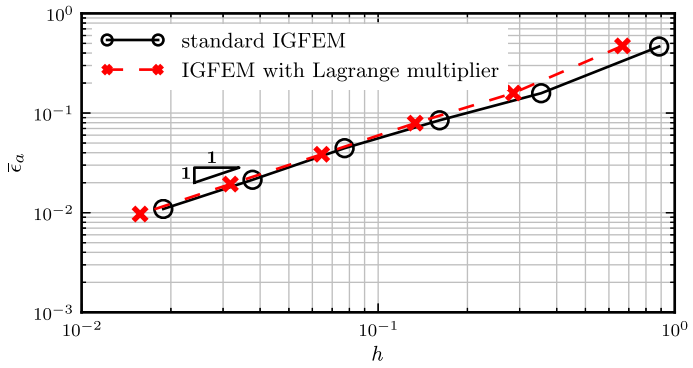

(b)

Figure 9. Convergence results for the Eshelby inclusion problem of Section 3.3. The figures show the error in the L^2-norm (a) and in the energy norm (b) as a function of the mesh size h.

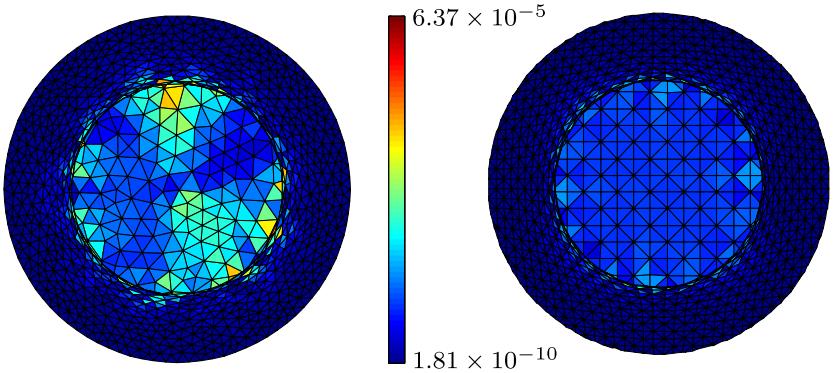

(a) (b)

Figure 10. Squared L^2-error in each element: (a) boundary conforming mesh and (b) non-conforming mesh.

By using the method presented in this paper, the burden of creating a mesh that conforms to the many surface asperities is avoided. Instead, the simple structured mesh shown in Figure 11(b) is used for the analysis.

Figure 12 shows the normal stress components σ_{11}, σ_{22}, together with the shear stress σ_{12}, on the deformed configuration for the given problem. It is worth noting that an arbitrary number of rough surfaces can be studied by using the same structured finite element mesh by just changing the roughness expressions of Equations (33).

DOI: 10.1002/nme

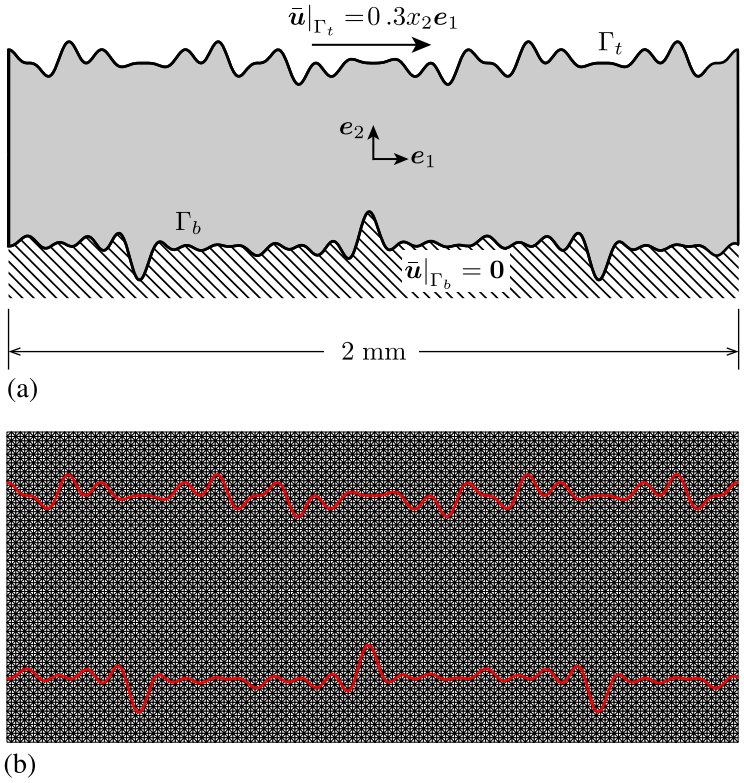

Figure 11. (a) Schematic of an epoxy film subjected to an imposed shear displacement on the top. (b) Structured non-matching mesh used for the analysis.

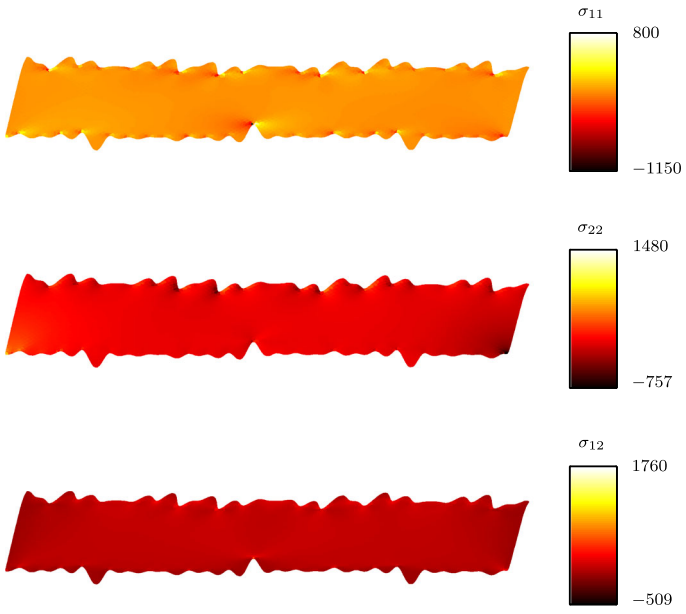

Figure 12. Deformed configuration and stress maps, in MPa, for the epoxy film problem outlined in Section 3.4. From the top to the bottom, the figures show the normal σ_{11}, σ_{22}, and the shear σ_{12} stress components.

DOI: 10.1002/nme

4. CONCLUSIONS

In this paper, a new formulation for the imposition of Dirichlet BCs for problems with complex boundary geometries was introduced. This method allows for the analysis of problems using non-matching FE meshes, thereby avoiding the burden of generating meshes that match the domain boundary. For this purpose, the IGFEM was combined with the Lagrange multiplier method, and the results show that the optimal rate of convergence is preserved. Because of the use of the IGFEM, the total number of DOFs should be smaller than the formulations that combine conventional XFEM/GFEM to enrich the primal space with a Lagrange multiplier field. Furthermore, no extra costs of identifying a stable Lagrange multiplier space are encountered. Even though the framework was presented in the context of linear elasticity, it is general and may be applicable to any type of elliptic linear boundary value problem where essential BCs need to be enforced. The method is robust and straightforward to apply. Furthermore, the versatility of the method permits the study of an arbitrary number of complex boundary geometries by using the same FE mesh, as demonstrated by the shearing of an epoxy film example of the previous section.

ACKNOWLEDGEMENTS

The financial support of the Swiss Federal Office of Energy within the project 'Multi-Scale Modeling of the Alkali-Silica Reaction' is gratefully acknowledged (Contract No. SI/500852-01). This research was also partially supported by the European Research Council ERCstg UFO-240332.

REFERENCES

1. Oden JT, Duarte CAM, Zienkiewicz OC. A new cloud-based hp finite element method. *Computer Methods In Applied Mechanics and Engineering* 1998; **153**(1-2):117–126.
2. Melenk JM, Babuska I. The partition of unity finite element method: basic theory and applications. *Computer Methods In Applied Mechanics and Engineering* 1996; **139**(1-4):289–314.
3. Babuska I, Melenk JM. The partition of unity method. *International Journal For Numerical Methods In Engineering* 1997; **40**(4):727–758.
4. Belytschko T, Black T. Elastic crack growth in finite elements with minimal remeshing. *International Journal For Numerical Methods In Engineering* 1999; **45**(5):601–620.
5. Belytschko T, Moes N, Usui S, Parimi C. Arbitrary discontinuities in finite elements. *International Journal For Numerical Methods In Engineering* 2001; **50**(4):993–1013.
6. Belytschko T, Gracie R, Ventura G. A review of extended/generalized finite element methods for material modeling. *Modelling and Simulation In Materials Science and Engineering* 2009; **17**(4):043001 (24pp).
7. Williams ML. The bending stress distribution at the base of a stationary crack. *Journal of Applied Mechanics* 1961; **28**(1):78–82.
8. Fries T-P. A corrected XFEM approximation without problems in blending elements. *International Journal For Numerical Methods In Engineering* 2008; **75**(5):503–532.
9. Ventura G, Moran B, Belytschko T. Dislocations by partition of unity. *International Journal for Numerical Methods in Engineering* 2005; **62**:1463–1487.
10. Moës N, Dolbow J, Belytschko T. A finite element method for crack growth without remeshing. *International Journal For Numerical Methods In Engineering* 1999; **46**(1):131–150.
11. Daux C, Moes N, Dolbow J, Sukumar N, Belytschko T. Arbitrary branched and intersecting cracks with the extended finite element method. *International Journal For Numerical Methods In Engineering* 2000; **48**(12):1741–1760.
12. Chessa J, Smolinski P, Belytschko T. The extended finite element method (XFEM) for solidification problems. *International Journal For Numerical Methods In Engineering* 2002; **53**(8):1959–1977.
13. Chessa J, Belytschko T. An extended finite element method for two-phase fluids. *Journal of Applied Mechanics-Transactions of the Asme* 2003; **70**(1):10–17.
14. Khoei AR, Nikbakht M. Contact friction modeling with the extended finite element method (X-FEM). *Journal of Materials Processing Technology* 2006; **177**(1-3):58–62.
15. Fish J, Yuan Z. Multiscale enrichment based on partition of unity. *International Journal For Numerical Methods In Engineering* 2005; **62**(10):1341–1359.
16. T-P F, Belytschko T. The extended/generalized finite element method: an overview of the method and its applications. *Inxing* 2010; **84**(3):253–304.
17. Lew AJ, Buscaglia GC. A discontinuous-Galerkin-based immersed boundary method. *International Journal For Numerical Methods In Engineering* October 2008; **76**(4):427–454.
18. Sanders JD, Dolbow JE, Laursen TA. On methods for stabilizing constraints over enriched interfaces in elasticity. *International Journal For Numerical Methods In Engineering* 2009; **78**(9):1009–1036.

DOI: 10.1002/nme

19. Moës N, Bechet E, Tourbier M. Imposing Dirichlet boundary conditions in the extended finite element method. *International Journal For Numerical Methods In Engineering* 2006; **67**(12):1641–1669.
20. Gerstenberger A, Wall WA. An embedded Dirichlet formulation for 3D continua. *International Journal for Numerical Methods in Engineering* 2010; **82**(5):537–563.
21. Babuska I. The finite element method with Lagrangian multipliers. *Numerische Mathematik* 1973; **20**(3):179–192.
22. Fernandez-Mendez S, Huerta A. Imposing essential boundary conditions in mesh-free methods. *Computer Methods In Applied Mechanics and Engineering* 2004; **193**(12-14):1257–1275.
23. Hautefeuille M, Annavarapu C, Dolbow J. Robust imposition of Dirichlet boundary conditions on embedded surfaces. *International Journal for Numerical Methods in Engineering* 2012; **90**:40–64.
24. Burman E, Hansbo P. Fictitious domain finite element methods using cut elements: I. A stabilized lagrange multiplier method. *Computer Methods In Applied Mechanics and Engineering* 2010; **199**:2680–2686.
25. Barbosa HJC, Hughes TJR. The finite element method with Lagrange multipliers on the boundary: circumventing the Babuška–Brezzi condition. *Computer Methods In Applied Mechanics and Engineering* 1991; **85**:109–128.
26. Nitsche J. Über ein Variationsprinzip zur Lösung von Dirichlet-Problemen bei Verwendung von Teilräumen, die keinen Randbedingungen unterworfen sind. *Abhandlungen aus dem Mathematischen Seminar der Universität Hamburg* 1971; **36**(1):9–15.
27. Hansbo A, Hansbo P. An unfitted finite element method, based on Nitsche's method, for elliptic interface problems. *Computer Methods in Applied Mechanics and Engineering* 2002; **191**(47-48):5537–5552.
28. Babuska I. The finite element method with penalty. *Mathematics of Computation* 1973; **27**:221–228.
29. Rangarajan R, Lew A, Buscaglia GC. A discontinuous-Galerkin-based immersed boundary method with non-homogeneous boundary conditions and its application to elasticity. *Computer Methods in Applied Mechanics and Engineering* 2009; **198**(17-20):1513 –1534.
30. Mergheim J, Kuhl E, Steinmann P. A hybrid discontinuous Galerkin/interface method for the computational modelling of failure. *Communications in Numerical Methods in Engineering* 2004; **20**:511–519.
31. Ji H, Dolbow J. On strategies for enforcing interfacial constraints and evaluating jump conditions with the extended finite element method. *International Journal For Numerical Methods In Engineering* 2004; **61**:2508–2535.
32. Mourad HM, Dolbow J, Harari I. A bubble-stabilized finite element method for Dirichlet constraints on embedded interfaces. *International Journal for Numerical Methods in Engineering* 2006; **69**(4):772–793.
33. Brezzi F, Fortin M (eds.) *Mixed and Hybrid Finite Element Methods*, Springer series in computational mathematics. Springer: Springer-Verlag New York Inc., 1991.
34. Béchet E, Moës N, Wohlmuth B. A stable Lagrange multiplier space for stiff interface conditions within the extended finite element method. *International Journal For Numerical Methods In Engineering* 2009; **78**:931–954.
35. Soghrati S, Aragón AM, Duarte CA, Geubelle PH. An interface-enriched generalized FEM for problems with discontinuous gradient fields. *International Journal for Numerical Methods in Engineering* 2012; **89**(8):991–1008.
36. Soghrati S, Geubelle PH. A 3D interface-enriched generalized finite element method for weakly discontinuous problems with complex internal geometries. *Computer Methods in Applied Mechanics and Engineering* 2012; **217–220**:46–57.
37. Soghrati S, Najafi AR, Lin JH, Hughes KM, White SR, Sottos NR, Geubelle PH. Computational analysis of actively-cooled 3D woven microvascular composites using a stabilized interface-enriched generalized finite element method. *International Journal Of Heat And Mass Transfer* 2013; **65**:153–164.
38. Soghrati S, Thakre PR, White SR, Sottos NR, Geubelle PH. Computational modeling and design of actively-cooled microvascular materials. *International Journal Of Heat And Mass Transfer* 2012; **55**:5309–5321.
39. Aragón AM, Soghrati S, Geubelle PH. Effect of in-plane deformation on the cohesive failure of heterogeneous adhesives. *Journal of the Mechanics and Physics of Solids* 2013; **61**(7):1600–1611.
40. Brenner SC, Scott RL. *The Mathematical Theory of Finite Element Methods*. Springer: New York, 2008.
41. Quarteroni A. *Numerical Models for Differential Problems*, MS&A. Springer: Milan, Berlin, New York, 2009.
42. Sukumar N, Chopp DL, Moës N, Belytschko T. Modeling holes and inclusions by level sets in the extended finite-element method. *Computer Methods in Applied Mechanics and Engineering* 2001; **190**(46-47):6183–6200.
43. Moës N, Cloirec M, Cartraud P, Remacle J-F. A computational approach to handle complex microstructure geometries. *Computer Methods in Applied Mechanics and Engineering* 2003; **192**(28-30):3163–3177.

DOI: 10.1002/nme